Title
Artificial Metalloproteins Containing Co4O4 Cubane Active Sites

Journal
Journal of the American Chemical Society, 140(8)

ISSN
0002-7863

Authors
Olshansky, Lisa
Huerta-Lavorie, Raúl
Nguyen, Andy I
et al.

Publication Date
2018-02-28

DOI
10.1021/jacs.7b13052

Peer reviewed

HHS Public Access

Author manuscript

J Am Chem Soc. Author manuscript; available in PMC 2018 March 23.

Published in final edited form as:

J Am Chem Soc. 2018 February 28; 140(8): 2739–2742. doi:10.1021/jacs.7b13052.

Artificial Metalloproteins Containing Co_4O_4 Cubane Active Sites

Lisa Olshansky[†], **Raúl Huerta-Lavorie**[‡], **Andy I. Nguyen**[‡], **Jaicy Vallapurackal**[†], **Ariel Furst**[‡], **T. Don Tilley**[‡,⊥], and **A. S. Borovik**[†]

[†]Department of Chemistry, University of California, Irvine, CA 92697

[‡]Department of Chemistry, University of California, Berkeley, CA 94720

[⊥]Chemical Science Division, Lawrence Berkeley National Laboratory, Berkeley CA 94720

Abstract

Artificial metalloproteins (ArMs) containing Co_4O_4 cubane active sites were constructed via biotin-streptavidin technology. Stabilized by hydrogen bonds (H-bonds), terminal and cofacial Co^{III}–OH_2 moieties are observed crystallographically in a series of immobilized cubane sites. Solution electrochemistry provided correlations of oxidation potential and pH. For variants containing Ser and Phe adjacent to the metallocofactor, $1e^-/1H^+$ chemistry predominates until pH 8, above which the oxidation becomes pH-independent. Installation of Tyr proximal to the Co_4O_4 active site provided a single H-bond to one of a set of cofacial Co^{III}–OH_2 groups. With this variant, multi-e^-/multi-H^+ chemistry is observed, along with a change in mechanism at pH 9.5 that is consistent with Tyr deprotonation. With structural similarities to both the oxygen-evolving complex of photosystem II (H-bonded Tyr) and to amorphous water oxidation catalysts (Co_4O_4 core), these findings bridge synthetic and biological systems for water oxidation, highlighting the importance of secondary sphere interactions in mediating multi-e^-/multi-H^+ reactivity.

TOC image

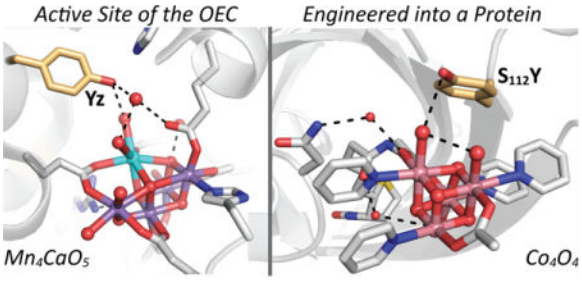

Oxygenic photosynthesis achieves the thermodynamically demanding oxidation of water by catalyzing a series of light-driven, proton-coupled electron transfer (PCET) events at a

Corresponding Author: aborovik@uci.edu, tdtilley@berkeley.edu.

Supporting Information

Synthesis and characterization of biotin conjugates; primer sequences and methods for Sav gene construction, expression and purification; XRD sample preparation, data processing, refinement statistics, electron and anomalous density and F_c–F_o omit maps; biot-β-Ala-**1** ⊂ 2×m-S_{112}F-Sav and biotin ⊂ 2×m-S_{112}Y-Sav structures; SWV sample preparation, control experiments, CV and optical measurements over 48 h, E_p and I_{max} values, and binding titration data are provided free of charge at http://pubs.acs.org.

Mn_4CaO_5 active site called the oxygen-evolving complex (OEC). In between the OEC and light-harvesting chlorophylls (P680) resides a tyrosine residue, referred to as Y_Z. By transforming electron transfer (ET) events at photooxidized $P680^{+\bullet}$ into PCET events at the OEC,[1] Y_Z circumvents the buildup of high energy intermediates during the $4e^-/4H^+$ oxidation of water to O_2. The global demand for inexpensive renewable energy brings to focus the elegance with which nature combines sunlight and water to make fuel. Artificial photosynthetic systems typically replace chlorophylls and the OEC with photoanodes and synthetic water oxidation catalysts (WOCs), respectively, but the challenge remains for the installation of PCET mediators like Y_Z capable of efficiently converting light-driven ET into PCET events. Positing such mediators proximal, but not directly coordinated to WOCs entails significant synthetic complexity. Additional challenges to catalyst design are the controlled synthesis of multinuclear metal complexes (capable of carrying out multi-e^- chemistry) that maintain exchangeable coordination sites for substrate water molecules to bind and which, for cost-effective strategies, function near pH-neutral conditions.

To address these challenges, we have employed biotinstreptavidin technology[2] to prepare ArMs in which biotinylated Co_4O_4 clusters are anchored within a protein (Sav) host. Featuring a μ_3–O cubane structural motif, the metallocofactor models aspects of the OEC, as well as of synthetic Co(O)(OH) WOCs.[3] We found that the host-guest interactions stabilize the Co_4O_4 core and were able to characterize these ArMs by single crystal X-ray diffraction (XRD). A series of ArMs were prepared that feature syn cofacial Co^{III}–OH_2 ligation, and in which mutagenesis of the surrounding protein host provides distinct secondary coordination sphere interactions to these ligands. The electrochemical properties across this series were examined by square wave voltammetry (SWV) as a function of pH. Correlating structure with function, our data suggest that an H-bond interaction between Tyr and a terminal Co^{III}–OH_2 gives rise to multi-e^-/multi-H^+ chemistry that is not operative in other ArM variants.

Scheme 1 depicts the structure of biot-β-Ala-**1**, a modified version of the tetranuclear $Co^{III}_4(\mu_3\text{–}O)_4(OAc)_4(py)_4$ complex (**1**). First prepared by Beattie,[4] and later characterized by Das and coworkers,[5] **1** has been well-studied as a dimensionally reduced model for active sites within Co(O)(OH) thin film WOCs.[6–12] Using recently reported ligand exchange methodologies,[13] equilibration of **1** and biot-β-Ala was followed by flash chromatography to provide the pure monobiotinylated species. Among the series of biotinylated cubanes prepared (SI), the β-alanine linker provided optimal binding within Sav. Additionally, two protein mutations were required; $K_{121}A$ to minimize steric interference, and $E_{101}Q$ to prevent the binding of metal clusters to the exterior of the protein. The $K_{121}A/E_{101}Q$-Sav variant used as the parent protein host will be referred to as 2×m-Sav herein. Additional modifications to the secondary coordination sphere were achieved through mutation of position 112. Across the series of variants: S_{112}, $S_{112}F$, and $S_{112}Y$ (2×m-Sav), titrations revealed stoichiometric binding of 4 equiv. biot-β-Ala-**1** per Sav tetramer (Figure S1).

Single crystals of biot-β-Ala-**1** ⊂ 2×m-Sav were generated following an *in crystallo* insertion protocol.[14] Figure 1a shows the structure of biot-β-Ala-**1** ⊂ 2×m-Sav to 1.46 Å resolution. Some ligand positions about the Co^{III} centers could not be modeled due to insufficient electron density likely caused by ligand rotation (about the Co—N_{py} axis) or exchange processes (at fluxional Co—OH_2 sites). In contrast to this dynamic behavior,

electron density for water molecules coordinated to the Co centers is observed in the data. Ligand exchange between acetate ions and water molecules occurs *in crystallo* to produce new types of cubanes that are stabilized within the protein host.

The *syn* coordination of two aqua ligands to Co1 and Co2 provide a relatively close O1···O2 distance of 2.62(4) Å. These aqua ligands are part of an ordered H-bonding network that we suggest aids in their stability. Protein residues S_{112} and G_{113}, as well as structurally conserved water molecules O3 and O6 contribute to the H-bonding network (Figure 1a). The H-bond between Co1 O1 and the O3 water molecule (O1···O3, 3.24(4) Å) is held in place by H-bonds to S_{112} and the O6 atom of water molecule (3.14(4) and 2.74(4) Å). The terminal Co1–O1 bond is 1.95(4) Å, which is slightly longer than the Co2–O2 bond length of 1.79(4) Å.

The placement of a metallocofactor within Sav also introduces asymmetry within the Co_4O_4 cube that is not present in the symmetrical parent complex **1**. For example, the acetate-bridged Co–O__Co angle of 93° in **1**[5] is compressed to 80° for the corresponding Co1__O__Co2 unit in biot-β-Ala-**1** ⊂ 2×m-Sav. This structural asymmetry evokes aspects of the OEC, where dynamic breathing modes associated with Mn–O–Mn bending and stretching are postulated to play a key role facilitating water oxidation.[15]

With the structure of biot-β-Ala-**1** ⊂ 2×m-Sav in hand, we sought to mutate Sav to place a Y close to the Co_4O_4 cluster, mimicking the positioning of Y_Z in PS II. Gratifyingly, solving the structure of biot-β-Ala-**1** ⊂ 2×m-S_{112}Y-Sav (Figures 1b and S3)[16] revealed a new H-bond between Y_{112} and O1. Comparison of the two structures reveals that both ArMs contain distinct H-bonds to terminally coordinated aqua ligands, including the same *syn*-aqua motif. In both cases, H-bonds between O4, O5, and the biotin carbonyl also stabilize terminal aqua ligation at Co4. However, in the biot-β-Ala-**1** ⊂ 2×m-S_{112}Y-Sav structure, one capping acetate is observed, bridging the Co2 and Co3 centers. Most intriguing about the biot-β-Ala-**1** ⊂ 2×m-S_{112}Y-Sav structure is the H-bond between Y_{112} and O1, which is assigned to a terminal Co–OH_2 moiety (O_Y···O1 = 3.07(5) Å). Relative to the corresponding Co1–O1 and Co2–O2 bonds in biot-β-Ala-**1** ⊂ 2×m-Sav, these bonds are elongated in 2×m-S_{112}Y-Sav to 2.17(5) and 2.08 (5) Å, respectively (Table S1). This change may be caused by the presence of a stronger H-bond interaction with Y112 relative to that with the O3 water in the biot-β-Ala-**1** ⊂ 2×m-Sav structure.[17]

Electrochemical experiments were performed with biot-β-Ala-**1** ⊂ 2×m-S_{112}X-Sav samples that were further purified using size exclusion chromatography. These samples were found to be stable in water for greater than 48 h as assessed by optical spectroscopy (Figure S4) and cyclic voltammetry (CV, Figure S5). Figure 2a presents SWV data collected with biot-β-Ala-**1** ⊂ 2×m-Sav as a function of pH. Unlike in the cases of **1** and biot-β-Ala-**1** (Figure S6),[12] oxidation of biot-β-Ala-**1** ⊂ 2×m-Sav is irreversible. CV data collected at multiple scan rates (5, 10, 50 mV/s) failed to produce a reverse, reduction wave. The observation of Nernst-like electrochemical behavior suggests that these events are rapid, and unlikely to affect analysis of the preceding oxidation.[18] Therefore, the potentials and pK_a values reported in Figure 2 are interpreted as apparent rather than true values derived from reversible equilibria. The pH-dependence of oxidation was explored over the range 6–11

because above pH 12, protein oxidation occurs, and below pH 5, Co is lost from the cluster. Control experiments were performed in which the working electrode after SWV was placed in fresh solution, and the experiment was repeated. Similarly, filtering post-run SWV samples through 10 kDa MWCO filters, the flow-through was re-subjected to the SWV conditions. In both cases, low current (maximally 18%) was observed and no clear features could be elucidated (Figure S7).

The plot of E_p vs. pH for biot-β-Ala-**1** ⊂ 2×m-Sav displayed in Figure 2b reveals a linear correlation with a slope of −63 ± 8 mV/dec up to pH 8. This slope is in-line with a $1e^-/1H^+$ (or $2e^-/2H^+$) oxidation, which would have a theoretical value of −59 mV/dec.[19,20] Above pH 8, E_p becomes pH-independent, suggesting there is an apparent pK_a at this value. Biot-β-Ala-**1** ⊂ 2×m-S_{112}F-Sav was found to have very similar electrochemical properties to biot-β-Ala-**1** ⊂ 2×m-Sav, exhibiting a slope of −63 ± 4 mV/dec up to pH 8, and then becoming pH-independent (Figure S8 and Table S2). The structure of biot-β-Ala-**1** ⊂ 2×m-S_{112}F-Sav (1.70 Å, Figure S9) shows a similar Co_4O_4 core to that of biot-β-Ala-**1** ⊂ 2×m-S_{112}Y-Sav but the aqua ligands do not interact with the F_{112} residue.

Complex **1**, as well as the biotinylated-Co_4O_4 cubane complexes (Table S3 and Figure S6), exhibit pK_as of 2.9–3.5,[12] and the related cubane $[Co_4O_4(OAc)_2(bpy)_4]^{2+}$ was shown to have a pK_a of 3.1 that corresponds to protonation of a bridging O^{2-} ligand.[21,22] Owing to the higher apparent pK_a observed here, the presence of terminal aqua ligands, and the similar pK_as reported for a dinuclear Co^{III}–OH_2 system,[23] we tentatively ascribe this PCET event to Co^{III}–$OH_2 \leftrightarrows Co^{IV}$–OH. If correct, this step is analogous to the pre-equilibrium reaction that has been observed in related thin film WOCs.[24] We note that the extent of charge delocalization within the singly oxidized cubane[9,11] remains unknown within the ArMs. Although desymmetrization of the cubane may favor a localized electronic structure,[9] the notation as Co^{IV}–OH is a formal oxidation state rather than a descriptor of the electronic structure.

Biot-β-Ala-**1** ⊂ 2×m-S_{112}Y-Sav, displays different electrochemical properties (Figures 2c and d) relative to biot-β-Ala-**1** ⊂ 2×m-Sav (Figures 2a and b) and ⊂ 2×m-S_{112}F-Sav (Figure S8). At pH values less than 9.5 (blue traces, Figure 2c), a slope of −38 ± 4 mV/dec is found, consistent with a $2e^-/1H^+$ event (theoretical value of −29 mV/dec). At pH values greater than 9.5 (purple traces, Figure 2c), a slope of −140 ± 10 mV/dec is observed, which is most consistent with a $1e^-/2H^+$ event (theoretical value of −118 mV/dec). From these data, we propose that Y_{112} engages in redox activity under the experimental conditions. To further explore this possibility, we performed SWV with biot-β-Ala ⊂ 2×m-S_{112}Y-Sav and biot ⊂ 2×m-S_{112}Y-Sav, proteins that lack a metallocofactor. At pH 10 we expected to observe $Y^-/Y^\bullet$ oxidation, and aimed to correlate this redox event with those observed in biot-β-Ala-**1** ⊂ 2×m-S_{112}Y-Sav. However, no redox activity was observed (Figure S10). Obtaining the structure of biotin ⊂ 2×m-S_{112}Y-Sav (1.36 Å, Figure S11), we found that in the absence of the metallocofactor, residue Y_{112} adopts a different orientation, placing it buried within the protein fold. The positioning of the phenolic residue limits accessibility, prohibiting SWV measurements.

The construction of ArMs provides opportunities for molecular control not possible in either fully synthetic or fully biological systems. For example, the metallocofactors within the biot-β-Ala-**1** ⊂ 2×m-S_{112}X-Sav family of ArMs maintain exchangeable coordination sites, enabling water to bind to some of the Co centers. Although common in biochemical systems, this type of substitution chemistry can be difficult to achieve synthetically because intermolecular reactions can occur. That two water molecules bind in a *syn*-fashion to adjacent Co centers is a significant discovery: this type of motif has been proposed as a key mechanistic intermediate in amorphous Co-WOCs,[12,23,25–27] where edge-site availability has been correlated with activity.[23,28,29]

Many enzymatic metallocofactors have Y residues within the secondary coordination sphere that mediate the flow of protons and electrons.[30] Duplicating these effects within synthetic systems is challenging because phenolic groups tend to coordinate to first-row transition metals. By using a protein host, we could install a phenol within the secondary coordination sphere of an immobilized metal cluster. In biot-β-Ala-**1** ⊂ 2×m-S_{112}Y-Sav, an H-bond is formed between Y and one of the aqua ligands, while direct coordination to the Co centers is avoided. Mutating this residue to F disrupts this H-bond and results in altered electrochemical properties.

A possible model fitting the electrochemical and crystallographic data is presented in Figure 3. Parts (a) and (b) illustrate a mechanism that is consistent with our data on biot-β-Ala-1 ⊂ 2×m-Sav; namely, the $1e^-/1H^+$, and $1e^-$ chemistry observed below and above pH 8, respectively. As noted earlier, the electronic structure of the oxidized cubane is unknown, and the Lewis structures of Figure 3 represent single resonance and tautomeric forms. Extended H-bond networks present in ArMs are also omitted. Figure 3c represents a mechanistic model for the type of chemistry that may be operative in biot-β-Ala-**1** ⊂ 2×m-S_{112}Y-Sav below pH 9.5. The potentials required to oxidized **1**[12] and neutral, protonated Ys,[31] are similar. This thermodynamic matching supports the possibility of electronic communication between the two redox-active centers. The presence of H-bonds between Co–OH_2 and Y, and between adjacent Co–OH_2 centers, support that redox cooperativity between the two sites may also be kinetically feasible. Above pH 9.5 (illustrated in Figure 3d) the potentials,[31] and Pourbaix slope become consistent with primarily $Y^-/Y^\bullet$ localized ET. The pK_a of Y can vary significantly in the protein environment,[32] but in the relatively open Sav pocket, and in the absence of interactions that would be expected to significantly perturb the Y_{112} pK_a (Figure 1b), we expect this value to be similar to that of the free amino acid and be close to 10.[33,34] Thus, we propose the change in mechanism at pH 9.5 signifies deprotonation of Y, and that above pH 9.5, Y_{112} is oxidized by ET rather than PCET.

The mechanistic insights gained through our studies highlight the precise balance that must be achieved between metallocofactors and PCET mediators in the design of artificial systems. In PS II, it is $Y_Z^\bullet$ that drives the oxidation and deprotonation of the OEC. Here, the potentials required for cubane oxidation are higher than that of Y_{112} and the flow of electrons is opposite to that in PS II. The dynamics observed here are more like those found in cyctochrome P450s, in which a nearby Y serves as an electron sink, protecting the active site from deleterious off-pathway oxidations.[35] Thus, the selection of Mn ions for biological water oxidation, and the optimum pH for enzymatic activity of 6.5,[36] coincide with Y-driven

PCET events.[37] If WOCs are to incorporate PCET relays playing a similar role to that of Y_Z, either a stronger oxidant than phenol, or WOCs requiring lower oxidation potentials[13] are needed. Notwithstanding, we have successfully installed a PCET mediator within the secondary coordination sphere of a "substrate"- bound multinuclear metal complex. Owing to this interaction, we observe multi-e^-, multi-H^+ reactivity not operative in other ArMs. By generating structure-function correlations at biomimetic metallocofactors, we begin to bridge the gap between molecular, materials, and biochemical systems for water oxidation.

Supplementary Material

Refer to Web version on PubMed Central for supplementary material.

Acknowledgments

The authors gratefully acknowledge generous gifts of biotin, codon-optimized pET24a-Sav plasmid, and iminobiotin-agarose resin from Prof. Thomas R. Ward. Prof. Matthew B. Francis and Jiang Wang are thanked for analytical instrumentation and helpful discussions. L.O. acknowledges the ACS Irving S. Sigal Postdoctoral Fellowship and A.S.B. acknowledges NIH (GM120349) for funding. T.D.T. thanks the U.S. DoE, Office of Basic Energy Sciences (Contract No. DE-AC02-05CH1123), R.H.-L. acknowledges the UC MEXUS-CONACYT Postdoctoral Fellowship, and A.L.F. acknowledges the A. O. Beckman Postdoctoral Fellowship.

References

1. Tommos C, Babcock GT. Acc Chem Res. 1998; 31:18–25.
2. Heinisch T, Ward TR. Acc Chem Res. 2016; 49:1711–1721. [PubMed: 27529561]
3. Kanan MW, Nocera DG. Science. 2008; 321:1072–1075. [PubMed: 18669820]
4. Beattie JK, Hambley TW, Klepetko JA, Masters AF, Turner P. Polyhedron. 1998; 17:1343–1354.
5. Chakrabarty R, Bora SJ, Das BK. Inorg Chem. 2007; 46:9450–9462. [PubMed: 17910439]
6. McAlpin JG, Surendranath Y, Dinca M, Stich TA, Stoian SA, Casey WH, Nocera DG, Britt RD. J Am Chem Soc. 2010; 132:6882–6883. [PubMed: 20433197]
7. McAlpin JG, Stich TA, Ohlin CA, Surendranath Y, Nocera DG, Casey WH, Britt RD. J Am Chem Soc. 2011; 133:15444–15452. [PubMed: 21913664]
8. Stich TA, Krzystek J, Mercado BQ, McAlpin JG, Ohlin CA, Olmstead MM, Casey WH, David Britt R. Polyhedron. 2013; 64:304–307.
9. Hadt RG, Hayes D, Brodsky CN, Ullman AM, Casa DM, Upton MH, Nocera DG, Chen LX. J Am Chem Soc. 2016; 138:11017–11030. [PubMed: 27515121]
10. Clatworthy EB, Li X, Masters AF, Maschmeyer T. Chem Commun. 2016; 52:14412–14415.
11. Brodsky CN, Hadt RG, Hayes D, Reinhart BJ, Li N, Chen LX, Nocera DG. Proc Natl Acad Sci. 2017; 114:201701816.
12. Nguyen AI, Ziegler MS, Oña-Burgos P, Sturzbecher-Hohne M, Kim W, Bellone DE, Tilley TD. J Am Chem Soc. 2015; 137:12865–12872. [PubMed: 26390993]
13. Nguyen AI, Wang J, Levine DS, Ziegler MS, Tilley TD. Chem Sci. 2017; 8:4274–4284. [PubMed: 29081963]
14. Mann SI, Heinisch T, Weitz AC, Hendrich MP, Ward TR, Borovik AS. J Am Chem Soc. 2016; 138:9073–9076. [PubMed: 27385206]
15. Pushkar Y, Yano J, Sauer K, Boussac A, Yachandra VK. Proc Natl Acad Sci U S A. 2008; 105:1879–1884. [PubMed: 18250316]
16. An additional structure of biot-β-Ala-1 ⊂ 2×m-S_{112}Y-Sav is also included in the SI (Figure S11, PDB# 6AUH). The major features of the two structures are similar, however we note that the higher resolution structure, which also contains stronger anomalous density for the four Co atoms (Figure S3), was obtained by including 1 mM Na_2IrCl_6 in the soaking buffer.

17. MacBeth CE, Gupta R, Mitchell-Koch KR, Young VG, Lushington GH, Thompson WH, Hendrich MP, Borovik AS. J Am Chem Soc. 2004; 126:2556–2567. [PubMed: 14982465]
18. Costentin C, Robert M, Savéant J-M. Phys Chem Chem Phys. 2010; 12:11179–111909. [PubMed: 20625575]
19. Pourbaix, M. Thermodynamics of Dilute Aqueous Solutions. Co., E. A. &, Ed.; London: 1949.
20. Pourbaix, M. Atlas of Electrochemical Equilibria in Aqueous Solutions. 1st. Pergamon Press Ltd.; New York: 1966.
21. Dimitrou K, Brown AD, Folting K, Christou G. Inorg Chem. 1999; 38:1834–1841. [PubMed: 11670955]
22. Symes MD, Surendranath Y, Lutterman DA, Nocera DG. J Am Chem Soc. 2011; 133:5174–5177. [PubMed: 21413703]
23. Ullman AM, Brodsky CN, Li N, Zheng SL, Nocera DG. J Am Chem Soc. 2016; 138:4229–4236. [PubMed: 26910289]
24. Surendranath, Y.; Kanan, M. W.; Nocera, D. G. **2010**, No. 14.
25. Surendranath, Y.; Lutterman, D. A.; Liu, Y.; Nocera, D. G. **2012**.
26. Wang LP, Van Voorhis T. J Phys Chem Lett. 2011; 2:2200–2204.
27. Li, X.; Siegbahn, P. E. M. **2013**, 13804–13813.
28. Du P, Kokhan O, Chapman KW, Chupas PJ, Tiede DM. J Am Chem Soc. 2012; 134:1–16. [PubMed: 22235988]
29. Farrow CL, Bediako DK, Surendranath Y, Nocera DG, Billinge SJL. J Am Chem Soc. 2013; 135:6403–6406. [PubMed: 23547707]
30. Gray HB, Winkler JR. Proc Natl Acad Sci. 2015; 112:10920–10925. [PubMed: 26195784]
31. Berry BW, Martinez-Rivera MC, Tommos C. Proc Natl Acad Sci. 2012; 109:9739–9743. [PubMed: 22675121]
32. Yokoyama K, Uhlin U, Stubbe J. J Am Chem Soc. 2010; 132:8385–8397. [PubMed: 20518462]
33. Kim K, Cole PA. J Am Chem Soc. 1998; 120:6851–6858.
34. Seyedsayamdost MR, Reece SY, Nocera DG, Stubbe J. J Am Chem Soc. 2006; 128:1569–1579. [PubMed: 16448128]
35. Yosca TH, Rittle J, Krest CM, Onderko EL, Silakov A, Calixto JC, Behan RK, Green MT. Science. 2013; 342:825–829. [PubMed: 24233717]
36. Berthold DA, Babcock GT, Yocum CF. Fed Eur Biochem Soc Lett. 1981; 134:231–234.
37. Tommos C, Tang X-S, Warncke K, Hoganson CW, Styring S, McCracken J, Diner B, Babcock GT. J Am Chem Soc. 1995; 117:10325–10335.

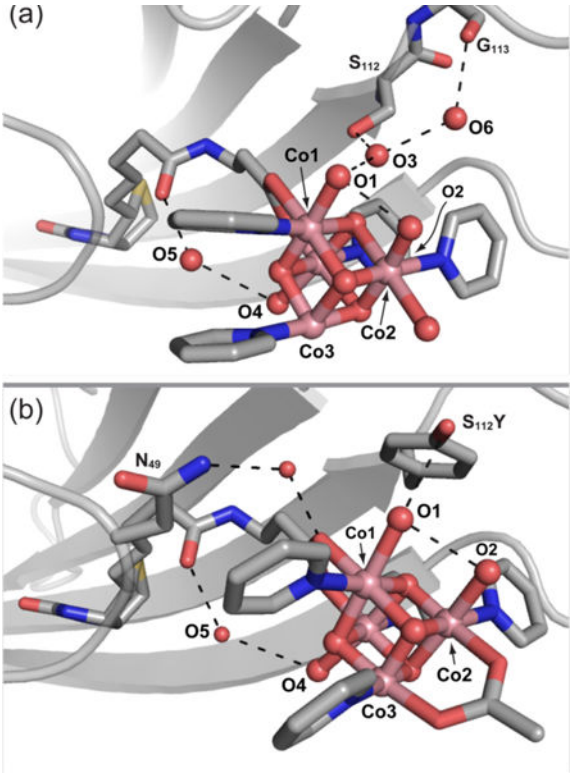

Figure 1.

Single crystal XRD structures of biot-β-Ala-**1**⊂ 2×m-Sav (1.46 Å, PDB 6AUC) (**a**), and biot-β-Ala-**1** ⊂ 2×m-S_{112}Y-Sav (1.36 Å, PDB 6AUE) (**b**). Electron and anomalous density, and F_c–F_o omit maps are provided in Figures S2 and S3.

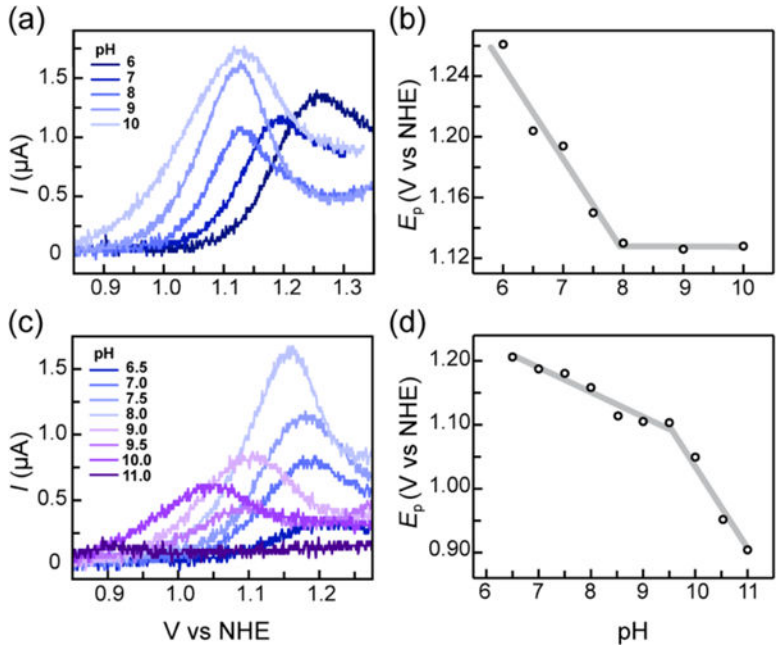

Figure 2.

SWV data collected with 2 mM biot-βAla-**1** ⊂ 2×m-Sav (**a**), the observed oxidation potentials (E_p) plotted as a function of pH (**b**), and the corresponding SWV data collected with 1 mM biot-β-Ala-**1** ⊂ 2×m-S_{112}Y-Sav (**c**), and E_p vs pH plot (**d**). In gray are least squares linear regression lines.

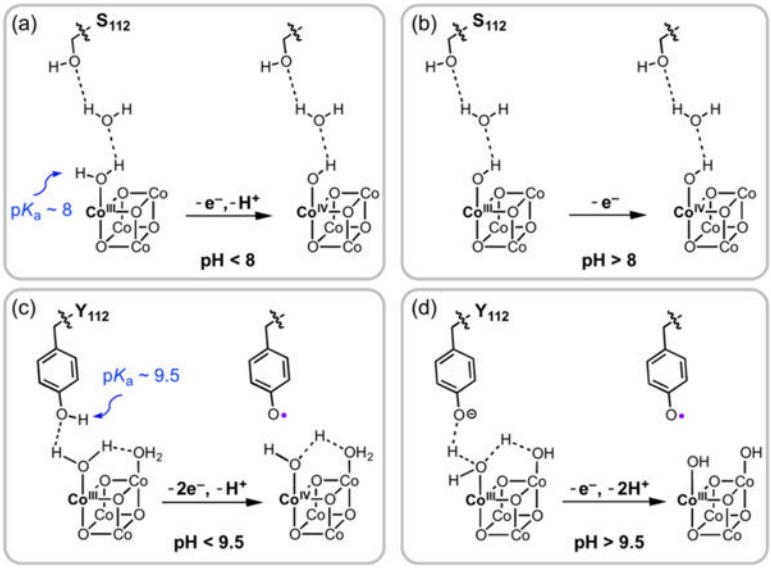

Figure 3.

Mechanistic model proposed to explain SWV and XRD data for 2×m-Sav (a and b) and S_{112}Y-2×m-Sav (c and d).

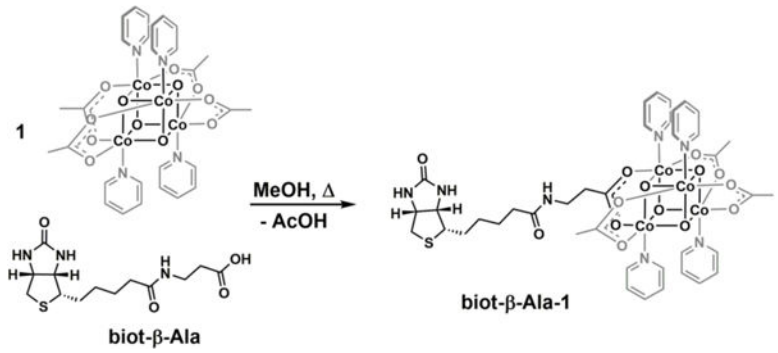

Scheme 1.
Synthesis of biot-β-Ala-1.